Numerical Investigation of Spray Combustion and Flow in LOX/H_2 Subscale Rocket Combustors

Hendrik Riedmann, Björn Kniesner*, Manuel Frey* and Claus-Dieter Munz***
**ASTRIUM GmbH Space Transportation, 81663 Munich, Germany*
Hendrik.Riedmann@astrium.eads.net, Bjoern.Kniesner@astrium.eads.net, Manuel.Frey@astrium.eads.net
***Institut für Aerodynamik und Gasdynamik, Universität Stuttgart, 70550 Stuttgart, Germany*
Munz@iag.uni-stuttgart.de

Abstract
For the validation of the in-house CFD tool Rocflam3, two different LOX/H2 subscale rocket combustors are investigated: the Mascotte single injector 10 bar test case [1] set up by ONERA and the ASTRIUM subscale chamber test case [2]. Rocflam3 solves the Favre Averaged Navier-Stokes equations and uses k-ϵ and k-ω turbulence modeling. In the presented cases turbulent combustion is treated via an equilibrium based presumed PDF approach with a mixture fraction formulation. A Lagrangian approach is applied for propellant droplet tracking and modeling the evaporation of the droplets. 2D/axisymmetric and three-dimensional simulations of both combustors have been performed. While the 2D results show good agreement with the experimental data, the 3D simulations require further investigations.

Nomenclature

Latin Symbols		
l^*	$[m]$	Characteristic length
$\dot{m}$	$[kg/s]$	Mass flow rate
O/F	$[-]$	Mixture ratio
p	$[bar]$	Pressure
Pr	$[-]$	Prandtl number
Sc	$[-]$	Schmidt number
T	$[K]$	Temperature

Greek Symbols		
ϵ	$[-]$	Contraction ratio
η	$[-]$	Mixture fraction
η_{c^*}	$[-]$	Combustion efficiency

Subscripts	
fu	Fuel
ox	Oxidizer
t	Turbulent quantity

Abbreviations	
CARS	Coherent Anti-Stokes Raman Scattering
CFD	Computational Fluid Dynamics
LES	Large Eddy Simulation
PDF	Probability Density Function
RANS	Reynolds Averaged Navier Stokes
SIMPLE	Semi Implicit Method for Pressure Linked Equations
SSME	Space Shuttle Main Engine

1. Introduction

Within the scope of validating the new 3D CFD tool Rocflam3 which is currently under development at Astrium Space Transportation in Ottobrunn as designated successor of the 2D/axisymmetric in-house code Rocflam-II [3], two different LOX/H2 subscale rocket combustors are investigated: the Mascotte single injector 10 bar test case [1] set up by ONERA and the ASTRIUM subscale chamber test case [2]. While for the Mascotte test case, main focus is put on computing the correct flame shape and flame temperatures, for the ASTRIUM test case the goal is to compute the correct wall heat flux. The Mascotte test case is a single injector test case which should give roughly comparable results no matter if treated with two- or three-dimensional CFD. The ASTRIUM subscale chamber is a multi-injector chamber where differences between the two- and three-dimensional results are to be expected.

Rocflam3 shall be able to compute combustion, flow and heat transfer in rocket combustion devices such as thrust chambers, preburners and gas generators in three spatial dimensions in order to support their industrial development and operation. Two-dimensional simulations shall be used for layout purposes while three-dimensional simulations shall serve for the final justification. Thereby, the computation time and effort must be appropriate for industrial application. To reach this goal, mainly well-known techniques are combined in this RANS code. Up to now, only a few test cases have been modeled with Rocflam3 and the validation process is still ongoing. An investigation of the Penn State single element combustor test case with Rocflam3 has been successfully performed earlier [4].
Since its presentation and discussion at the Rocket Combustion Modeling Workshop in 2001 [5], the Mascotte 10 bar test case has been investigated by numerous authors with different numerical approaches. All of them use RANS methods as is the case in the present work. While the results shown by most authors are based on axisymmetric simulations, Scherrer et al. [6] and Lempke et al. [7] consider the real three-dimensional configuration. In the present work, results are shown for both 2D/axisymmetric and 3D simulations. Scherrer et al. [6], Lempke et al. [7], Izard & Mura [8], Ivancic et al. [9] as well as the authors of this work use mixed Euler-Lagrange approaches, whereas Farmer et al. [10] use an Euler-Euler approach. Chen et al. [11] apply single-phase combustion modeling not taking into account droplet dynamics. Despite using different approaches, all of the cited authors show satisfying results with regard to their individual objectives.
The ASTRIUM subscale chamber test case has been presented at the Rocket Combustion Modeling Workshop in 2006 [12]. Apart from the contributions to that workshop, there are only a few publications on this test case. Ivancic et al. [9], [13] and Frey et al. [14] show comparisons between two- and three-dimensional simulations obtained with the ASTRIUM in-house code Rocflam-II and a commercial CFD tool, respectively. While both tools use RANS methods, Rocflam-II employs an Euler-Lagrange approach to treat the transcritical oxygen injection. However, both tools provide good agreement with the experimental data. Masquelet [15] shows an attempt of the unsteady, three-dimensional LES simulation of this test case but is not able to achieve good agreement with the measured heat flux.
In this paper, the applied modeling approach is described shortly in section 2. The simulation of the Mascotte test case is discussed in section 3 whereas the simulation of the ASTRIUM subscale chamber test case is presented in section 4. A short conclusion is given in section 5.

2. Modeling Approach

For the simulation of the two-phase flow test cases treated in this work, an Euler-Lagrange approach is applied. The continuous gas phase is treated using an Euler description, solving the Favre-averaged conservation equations for mass, momentum and enthalpy in three spatial dimensions. The equations are discretized with a Finite-Volume scheme for non-orthogonal, boundary-fitted and block-structured grids according to the pressure based SIMPLE algorithm described by Patankar & Spalding [16]. The resulting system of partial differential equations is solved using Stone's strongly implicit procedure [17]. Assuming that steady state solutions for both test cases exist, the transient terms, (i.e. the time derivatives) in the conservation equations are set to zero before solving the system of equations.
Three different turbulence models are applied in this work: A comparison between the Wilcox k-ω model [18] and the standard k-ϵ model [19] is shown for the Mascotte test case whereas a 2-layer k-ϵ model as described by Rodi [20] is used for the ASTRIUM subscale chamber test case. This 2-layer model employs the standard k-ϵ model in the core flow and switches to a one-equation model in the vicinity of the wall thereby enabling a decent computation of the boundary layer flow and the wall heat flux. As no wall heat flux measurements are available for the Mascotte test case just the standard high Reynolds modeling is used there. All three turbulence models require solving transport equations for the turbulent kinetic energy k and its dissipation ϵ or dissipation per unit turbulent kinetic energy ω, respectively. The Durbin realizability constraint [21] has been applied in both models to limit the eddy viscosity.
In order to account for the interaction between turbulence and chemistry, an equilibrium based presumed PDF approach is applied. The thermodynamic and transport properties obtained for chemical equilibrium are superposed with a one-dimensional Beta-PDF for the mixture fraction and then integrated over the mixture fraction range. Therefore, additional transport equations are solved for the mixture fraction and its variance. The computed values for enthalpy, pressure, mixture fraction and mixture fraction variance are used for a table lookup of the integrated quantities. These quantities are temperature, density, molar mass of the mixture, heat conductivity, specific heat capacity, viscosity, species concentrations and the derivative of pressure with respect to density.
In the present work, the injection of both hydrogen and oxygen is always treated via the Lagrangian module for propellant droplet tracking and evaporation as described by Kniesner et al. [22]. This module is a part of Rocflam3 which is loosely coupled to the Euler module. The treatment of the injected propellants depends on their thermodynamic states, i.e. it is distinguished between sub-, trans- or supercritical injection. Propellants injected in sub- or transcritical state are tracked throughout the flow field until vaporized. Thereby, they interact with the gas phase by releasing mass, momentum and enthalpy which are transferred via source terms in the conservation equations. There are no extra source terms in the transport equations of the turbulent quantities. However, there is of

course an influence on turbulence via the changes in the velocity components. The droplet trajectories are computed based on the solution of the gaseous flow field. Propellants injected in supercritical state are completely transferred to the continuous gas phase at their injection locations via source terms in the conservation equations. One background for this approach to treat supercritical propellants is to get rid of the requirement for the computational grid to resolve the injectors exactly in order to be able to achieve the correct combination of mass flow and momentum. Both quantities can be specified independently of each other when using the Lagrange module. This offers the possibility to simulate different injector configurations with only one grid, which has shown to be a great advantage for the industrial application. Another advantage becomes clear when thinking of the axisymmetric simulation of a multi-injector chamber such as the ASTRIUM subscale chamber, where rows of injection elements have to be modeled as rings: there one can specify both the correct mass flow and momentum while preserving the distance between injection element and wall with this approach.
To keep the computational effort low, not every single droplet of the injected propellant is tracked but only a certain number of representative trajectories is computed. Therefore, discrete diameters and injection angles are defined and assigned with specific probabilities. For the propellant droplet tracking procedure, an equation of motion must be solved for each droplet parcel. Droplet vaporization is approximated using the model by Abramzon & Sirignano [23].

3. Mascotte Single Element Combustor

3.1 Hardware and Test Data

The Mascotte 10 bar test case has been described in detail by Vingert & Habiballah [1]. Nevertheless, a short description shall be given here. The Mascotte combustor works at a chamber pressure of $p_c = 10bar$ and a mixture ratio of $O/F = 2.11$. The chamber has one shear-coaxial injector located on the center axis. Liquid oxygen is injected in the core of the injector at a temperature of $T_{ox} = 85K$ whereas the surrounding hydrogen is injected in gaseous state at $T_{fu} = 287K$. The oxygen mass flow rate is $\dot{m}_{ox} = 50\,g/s$ and the hydrogen mass flow rate is $\dot{m}_{fu} = 23.7\,g/s$. The diameter of the oxygen tube is $5mm$ and the diameters of the hydrogen annulus are $5.6mm$ and $12mm$. A sketch of the Mascotte combustor is shown in Figure 1. The chamber has a square cross section with an edge length of $50mm$. The distance between the injector and the throat is $478mm$. The throat diameter is $15mm$. For the purpose of optical diagnostics the chamber is equipped with helium-cooled quartz windows on two sides. Liquid nitrogen is used to cool down the oxygen before injection.

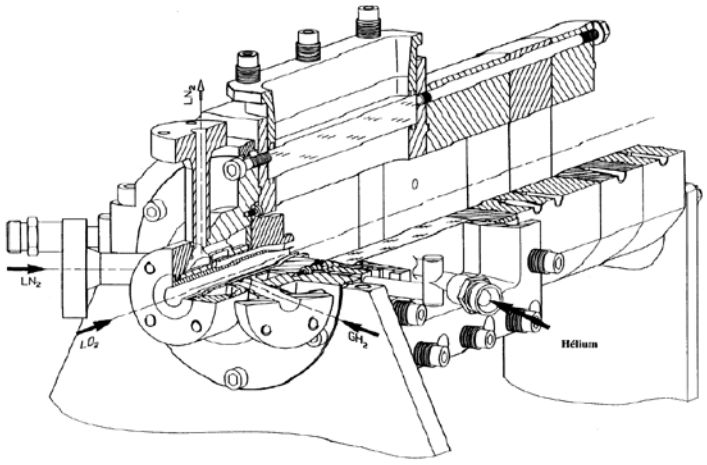

Figure 1: Sketch of the Mascotte combustor (taken from [1])

One should have in mind that neither the operation point (combination of chamber pressure and mixture fraction) of the Mascotte test case nor the geometry of the chamber is representative for common rocket engines. The area ratio between chamber and throat is $\epsilon = 14.1$ and the characteristic chamber length is $l^* = 6.6m$. Both values are notably higher than they are for common rocket engines like for example the SSME, Vulcain and HM7. For those engines, contraction rates in the order of $\epsilon \approx 2.5 - 3$ and characteristic lengths of $l^* \approx 0.7m - 0.8m$ can be found. The characteristic chamber length has an influence on the combustion efficiency via the residence time of the propellants in the combustion chamber. For a good H_2/O_2 injection system, a combustion efficiency of $\eta_{c^*} > 0.98$ can be reached with a characteristic length of $l^* = 0.6m$. For mass reasons, the characteristic length will always be chosen as small as possible but as high as necessary as there is a trade between performance and engine mass. These

thoughts about the chamber dimensions are described here just in order to highlight that the Mascotte combustor is not really comparable to common rocket thrust chambers. Nevertheless, it is a very interesting and well reported test case to investigate the combustion of cryogenic propellants which is the reason why it has been chosen for this work.
Several authors have published on the experimental investigation of the Mascotte combustor. The experimental data which are used for comparison with the numerical results in this work originate from two publications: There is an Abel-transformed emission image and mean temperature profiles published by Candel et al. [24] as well as additional mean temperature profiles published by Grisch et al. [25]. The emission images are shown in Figure 2. The left picture shows the average emission image whereas the right picture shows the Abel-transformed emission image which is suited to be compared with isoplots of the temperature or the OH concentration from numerical simulations. The temperature measurements have been obtained by CARS thermometry. The mean temperature values, the measurement locations, the standard deviations and the validation rates are illustrated in Figure 3. The validation rate is defined as the "ratio between the number of (CARS) spectra successfully processed and the total number of laser shots during a run" [25]. The standard deviation is induced by turbulent fluctuations and must not be mixed up with the measuring uncertainty as that one is much lower. Although being highly turbulent, the combustion process is said to be stationary in both cited publications which is a main requirement for the RANS simulations presented in this work.

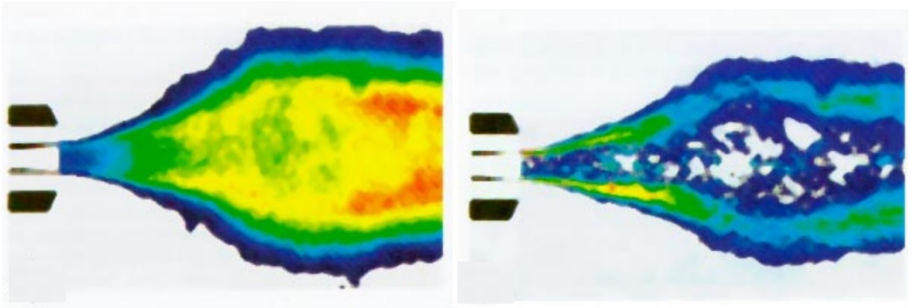

Figure 2: Average OH emission image (left) and Abel-transformed emission image (right) (taken from [24])

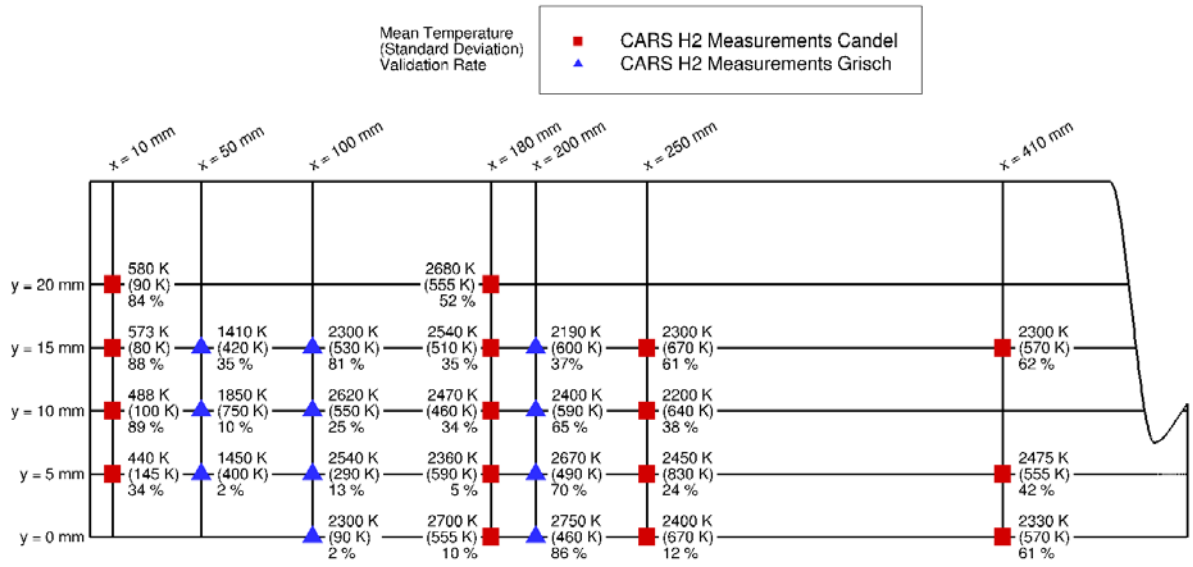

Figure 3: Mean temperatures obtained by CARS thermometry – values gathered from two publications: Candel et al. [24] and Grisch et al. [25]

3.2 Simulation Settings

As Rocflam3 has a three-dimensional solver which requires a three-dimensional grid, the 2D/axisymmetric computations are performed on a segment of one degree with one grid cell in circumferential direction. In axial direction, a constant cell width of $0.5mm$ is applied in the cylindrical part of the chamber with a refinement down to

$0.1mm$ in the throat area. No grid refinement has been used at the faceplate. In radial direction, the grid starts with a resolution of $0.4mm$ in the main flow and ends with a cell width of $50\mu m$ at the chamber wall, i.e. there is a refinement in the boundary layer. With these dimensions, the grid consists of a total number of $1054 \times 100 = 1.054 \cdot 10^5$ grid cells. It is shown in Figure 4.
Vingert & Habiballah [1] propose the injection of the oxidizer droplets on a conical solid boundary resolved by the grid to represent the liquid oxygen core. This has not been done here to keep the computational grid as simple as possible. Thereby, the suitability of this approach for a future application in multi-injector configurations is validated. Since multi-injector configurations are subject of industrial work, methodologies used for validation on subscale level (see also [3], [22]) have to be transferable to full-scale simulations. Both the faceplate and the liner wall are modeled as adiabatic no-slip walls. Symmetry boundary conditions are applied in circumferential direction. A supersonic boundary condition is set on the outlet.

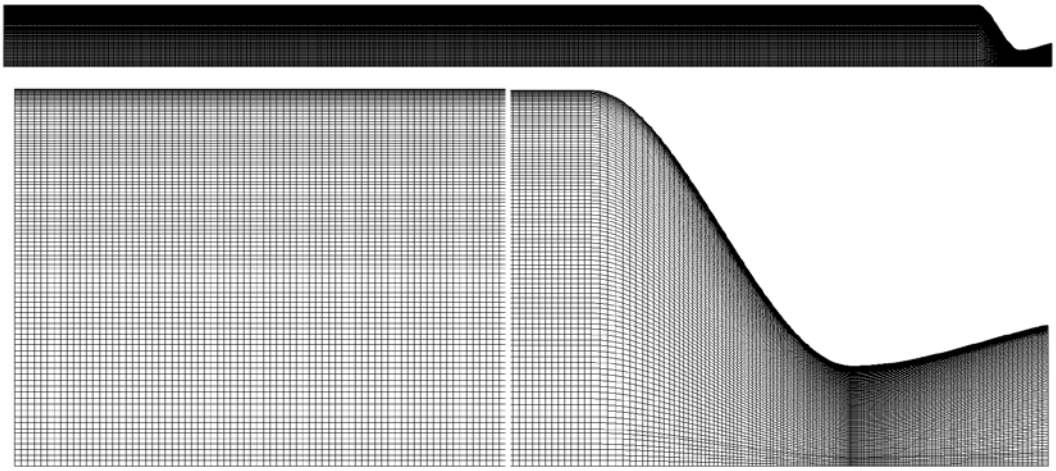

Figure 4: Mascotte 10 bar test case 2D/axisymmetric simulation – computational grid (top: complete domain, bottom left: zoom on the inflow and faceplate region, bottom right: zoom on the throat region)

As proposed by Vingert & Habiballah [1] the oxygen droplet size distribution is modeled using a Rosin-Rammler distribution with a mean diameter of $130\mu m$. In the simulation, this distribution is approximated using 25 discrete droplet sizes. The injection velocity is $2.18\,m/s$ as given by Vingert & Habiballah [1]. The droplets enter the domain along 30 discrete vectors with off-axis angles between 0° and 15°. The injection of the droplets is distributed over six grid cells. With these settings, the spray is modelled by 4500 representative trajectories each covering a certain number of real oxygen droplets. Droplets hitting the wall perform an elastic collision with it and are reflected.
As explained in Chapter 2, the gaseous hydrogen is brought into the domain in a similar way as the liquid oxygen, i.e. by the Lagrangian droplet tracking module. However, it is transferred from the Lagrangian to the Eulerian regime immediately via source terms for mass, momentum and enthalpy. The injection velocity of the hydrogen is $319\,m/s$.
In the two-dimensional case, the Wilcox k-ω model [18] and the standard k-ϵ model [19] are compared. The k-ω model is used in combination with the improved near wall treatment as described by Menter et al. [26]. The turbulent quantities are $Pr_t = 0.9$ and $Sc_t = 0.6$. These values have shown to give good agreement with experimental data for the Penn State test case [4] and therefore have been adopted here.
For the three-dimensional simulation, the simulation settings are basically the same as for the 2D/axisymmetric simulation. Of course, the grid is different and also - due to the injector being resolved by a larger number of grid cells - the number of representative trajectories is higher. There is no boundary layer refinement in this case in order to keep the number of grid cells lower. This should work fine in combination with the applied High Reynolds k-ϵ model. The grid consists of a total number of about $1.6 \cdot 10^6$ grid cells and the spray is modeled by 23500 representative trajectories.

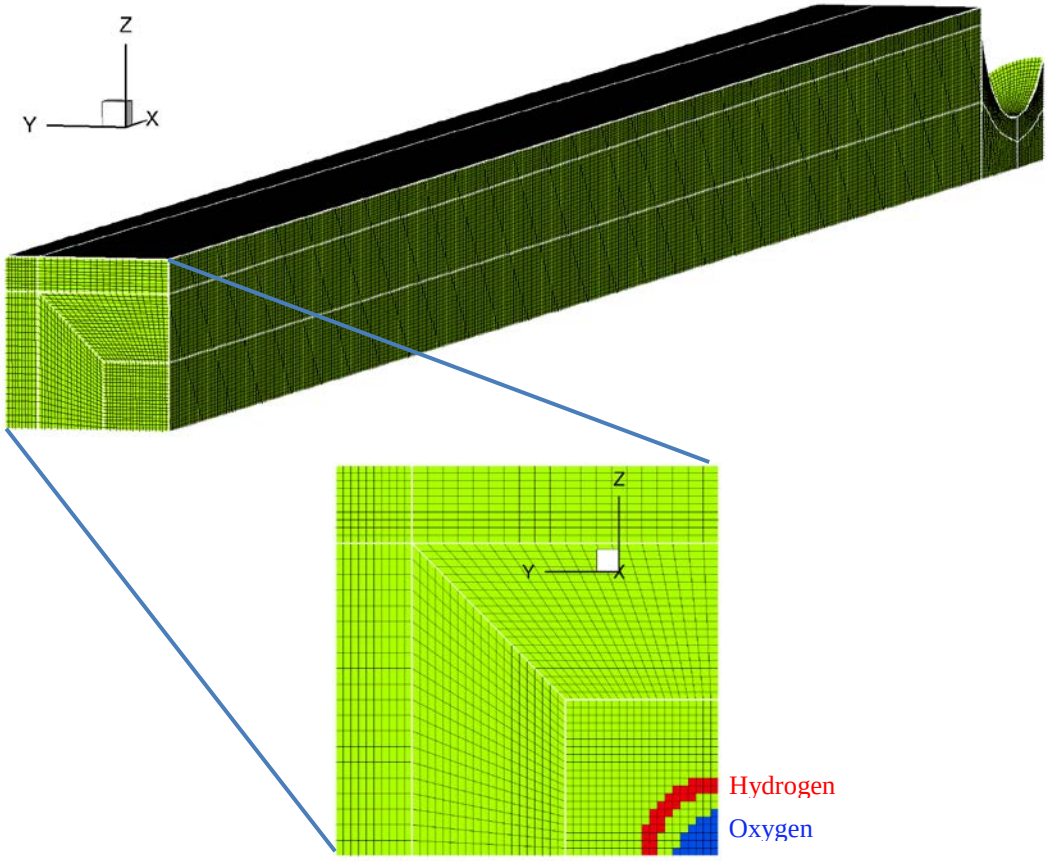

Figure 5: Mascotte 10 bar test case 3D simulation - computational grid

3.3 Simulation Results

3.3.1 2D/axisymmetric simulations

Figure 6 shows the temperature field and the streamlines for the 2D/axisymmetric simulation as well as the mean temperatures from CARS thermometry. Results obtained with the k-ω model and the k-ϵ model are compared. As one expects, there is a pair of vortices in the corner between faceplate and liner: a large one and a small counter-rotating one. The larger vortex borders the flame on the one side and on the other side there is a colder region around the symmetry axis where most of the oxygen evaporates. The flame itself starts very thin and widens in flow direction. As can be seen by the shape of the streamlines crossing the hot zone, there is a strong expansion in the flame. Downstream of $x \approx 0.2m$ the streamlines are almost parallel down to the convergent part of the chamber. In the flame region noticeable differences between the two turbulence models can be observed. The flame temperature is much higher for the k-ω model and also the flame shapes are different. As can be seen in Figure 7 where the turbulent kinetic energy is visualized, these effects can be attributed to differences in the turbulent kinetic energy. Using the PPDF chemistry model a higher turbulent kinetic energy leads to a higher mixture fraction variance which in turn leads to a lower combustion temperature. Comparing the numerical results in Figure 6 with the mean temperatures from CARS thermometry the agreement seems to be poor especially in the flame. However, it is worth also to take into account the standard deviations of the experimental values. More quantitative illustrations are therefore shown in Figure 10 and Figure 11. Another effect which is visible in Figure 7 and should be mentioned shortly is that the k-ϵ model overestimates the turbulent kinetic energy in the divergent part of the nozzle although the Durbin realizability constraint [21] has been applied with both models.

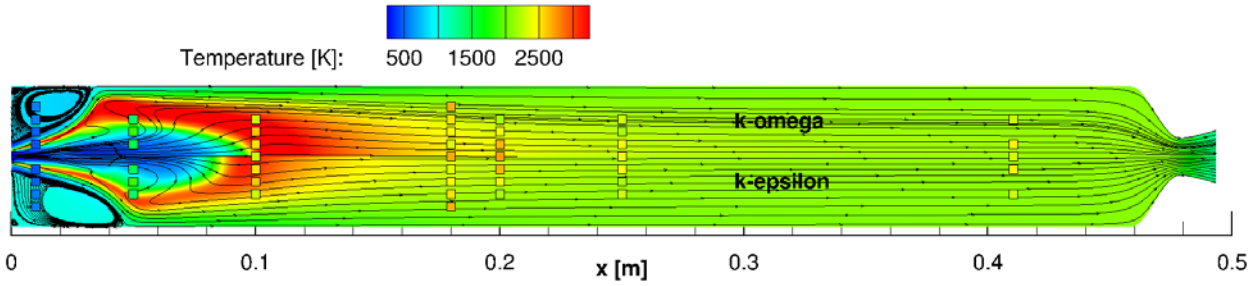

Figure 6: Mascotte 10 bar test case 2D/axisymmetric simulation – temperature field, streamlines and mean temperatures from CARS thermometry (small boxes). Upper side: k-ω model, lower side: k-ϵ model

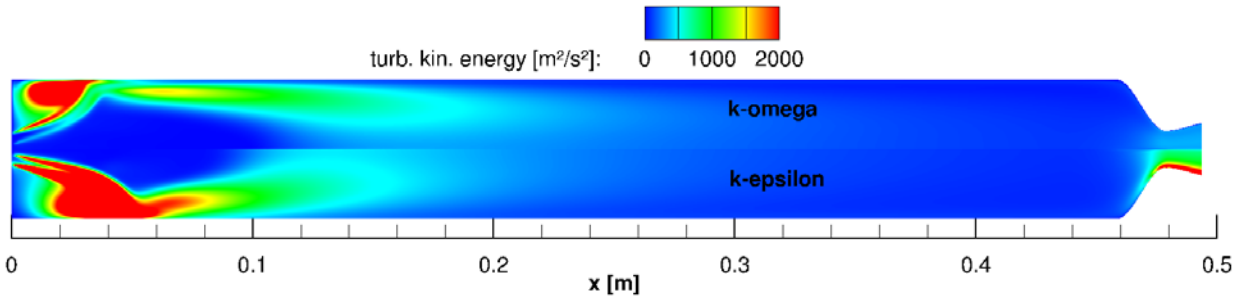

Figure 7: Mascotte 10 bar test case 2D/axisymmetric simulation – turbulent kinetic energy. Upper side: k-ω model, lower side: k-ϵ model

Figure 8 shows the mass source terms that are transferred from the Lagrangian spray model to the gaseous phase. The small peak at the faceplate corresponds to the hydrogen which enters the gaseous phase immediately. All the rest corresponds to the evaporation of the oxygen. Looking at the k-ω model results one can see clearly that droplets hit the wall and are reflected. Due to the different flame shapes this effect is not visible for the k-ϵ results. There is no other droplet wall interaction model implemented in Rocflam3 yet. At $x \approx 0.04m$ for the k-ϵ model and at $x \approx 0.02m$ for the k-ω model there are interesting peaks in the mass source terms. These peaks relate to the flow deflection which can be observed there by looking at the streamlines. This deflection is caused by the strong expansion of the flow in the flame. One can see that the evaporation is almost completed at $x \approx 0.2m$.

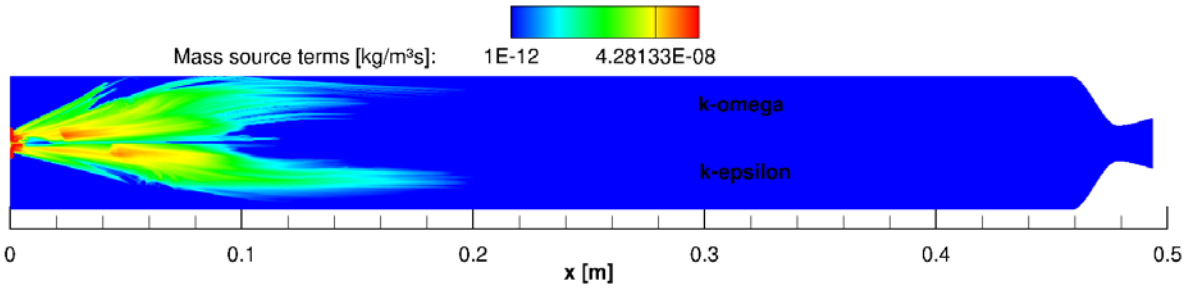

Figure 8: Mascotte 10 bar test case 2D/axisymmetric simulation – mass source terms from hydrogen and oxygen. Upper side: k-ω model, lower side: k-ϵ model

Figure 9 shows a comparison between the computed OH concentration fields for both turbulence models and the Abel-transformed emission image from the experiment. Please note that the lower side of the emission image (see Figure 2) is used for this comparison and that the upper and lower sides are not identical. Analyzing the differences between the numerical and the experimental results, one can see that the qualitative agreement is a bit better for the k-ϵ model. However, even that one does not agree with the experimental data perfectly. The cold region around the chamber axis is still smaller in the experiment than in the simulation, i.e. the flame expands a bit more in the simulation. The different OH concentrations in the numerical results are caused by the differences in the temperature and mixture fraction variance fields.

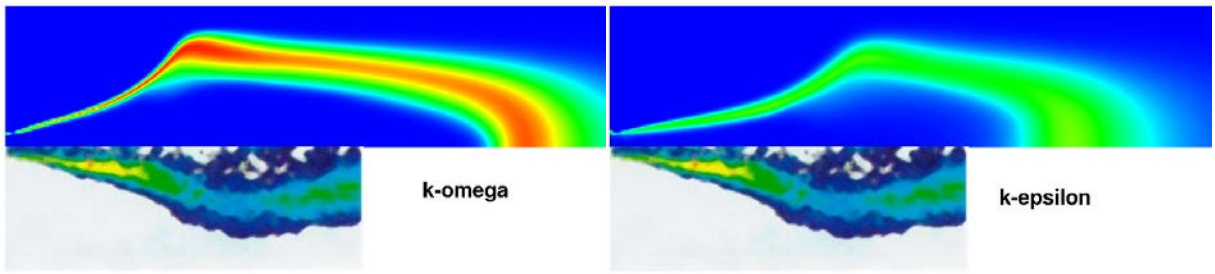

Figure 9: Mascotte 10 bar test case 2D/axisymmetric simulation – comparison between experimental and numerical results regarding the flame structure. Upper side: OH concentration from simulation, lower side: OH emission from test. Left: k-ω model, right: k-ϵ model

To make some quantitative judgments it is necessary to compare the simulation results with the mean temperatures obtained by CARS thermometry. For that purpose, experimental results from two different publications ([24] and [25]) are available. Figure 10 shows the numerical and the experimental results for four radial positions where measured temperatures exist. The general agreement between numerical and experimental results looks quite good and at the most locations the differences between the two turbulence models are smaller than the standard deviation of the experimental data. While there are some points where the agreement between simulation and experiment is nearly perfect, there are some other points where the agreement is much worse, i.e. there is no homogeneous behavior. The flame core length appears to be better reflected by the k-ω model while the k-ϵ model slightly underestimates it (see Figure 10, plot for $y = 0mm$).

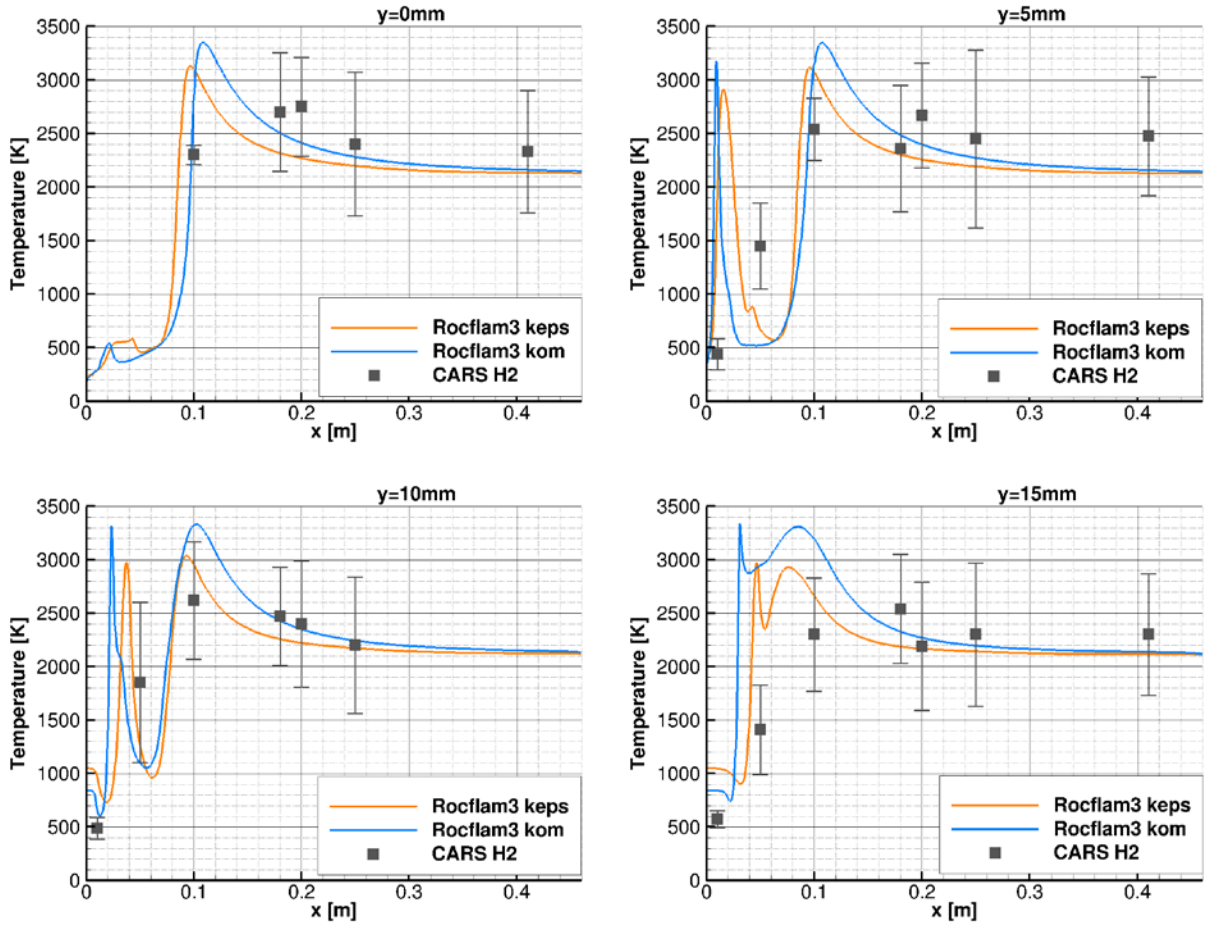

Figure 10: Mascotte 10 bar test case 2D/axisymmetric simulation– comparison between experimental and numerical results regarding local temperatures for different radial positions

Figure 11 shows the numerical and the experimental results for four different axial positions. While the experimental results are taken from Candel [24] and Grisch [25] is indicated by the shape and color of the symbols (compare to Figure 3). The first axial position is at $x = 10mm$, i.e. very close to the faceplate where the vortices reside and the flame starts to spread. While the experimental data gives values between $440K$ and $580K$ with quite small standard deviations, both numerical results show a strong peak of about $3000K$ caused by the flame and nearly constant temperatures for $y > 10mm$ which are notably higher than the measured ones. It shall be remarked that taking into account the good agreement between the numerical and experimental data regarding the emission images, one definitely expects a temperature peak at some radial position at $x = 10mm$ which the CARS thermometry does not resolve. At $x = 50mm$ the agreement is not really good for both turbulence models but it becomes better at $x = 100mm$. While the temperature close to the axis is underestimated at $x = 50mm$, it is overestimated at $x = 100mm$. The strong temperature rise in the flame which is visible in the numerical results at $x = 50mm$ is not visible in the experimental results. From the numerical point of view, this difference may either be caused by a too fast mixing or by the assumption of chemical equilibrium being unsuitable here. However, there may also be some inaccuracies in the experimental data as again no clear flame front can be identified. At $x = 180mm$, which is not shown here, the experimental data shows a strange behavior: the temperature first decreases and then increases with increasing radial position. This is contradictory to the behavior that can be seen at $x = 250mm$ (shown here) and $x = 410mm$ (not shown here). Farmer et al. [10] also discuss this possible inconsistency in the experimental data and criticize that error bounds are missing. The simulations compute a monotone temperature decrease with increasing radial position for those three axial positions. Nevertheless, the temperature levels computed in the simulation fit quite well with the measured ones for those positions.

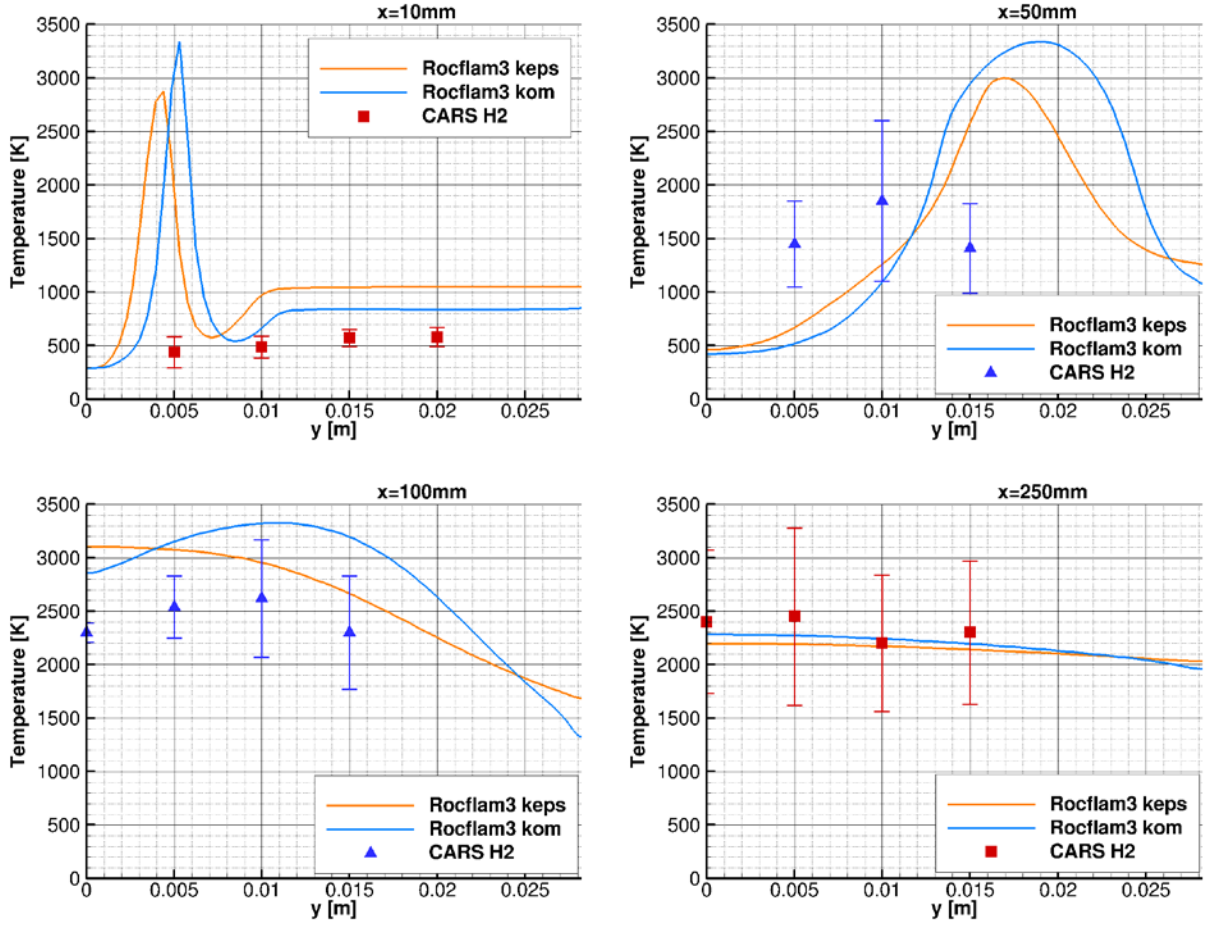

Figure 11: Mascotte 10 bar test case 2D/axisymmetric simulation– comparison between experimental and numerical results regarding local temperatures for different axial positions

To draw a conclusion from the shown 2D/axisymmetric results, one can say that the agreement between simulation and experimental data is satisfactory. While the flame shapes agree well between the experiment and the k-ϵ model simulation, a better agreement would be desirable for the k-ω model. Although the comparison of the flame shapes makes the k-ϵ model look better, no clear favorite can be chosen from the comparison of the local mean

temperatures. Some of the mean temperatures, e.g. at the axial position $x = 10mm$, expose systematic differences between numerical results and experimental data which should be addressed in future work.

3.3.2 Three-dimensional simulation

Figure 12 shows the temperature field for the three-dimensional simulation. It is noticeable that the flame is longer than in the 2D/axisymmetric simulation while the general flame shape looks similar. As visible in Figure 13, where slices of the temperature field at discrete axial positions are shown, the flow is not axisymmetric in the three-dimensional simulation. Instead, the square cross section of the chamber can be recognized in the flame shape. This is an interesting phenomenon whose detailed investigation shall be addressed in future work. As a grid study for the three-dimensional case has not been performed yet, an influence of the computational grid cannot be excluded at the moment. Therefore, no further analyses of the three-dimensional results are discussed here. However, this simulation demonstrates the general capability of Rocflam3 to simulate combustion problems in three spatial dimensions.

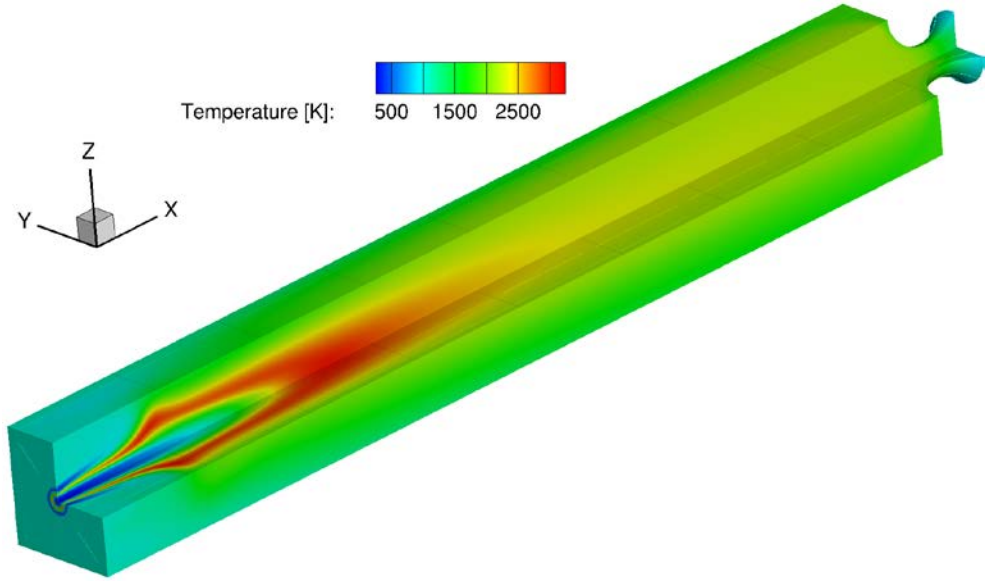

Figure 12: Mascotte 10 bar test case 3D simulation – temperature field

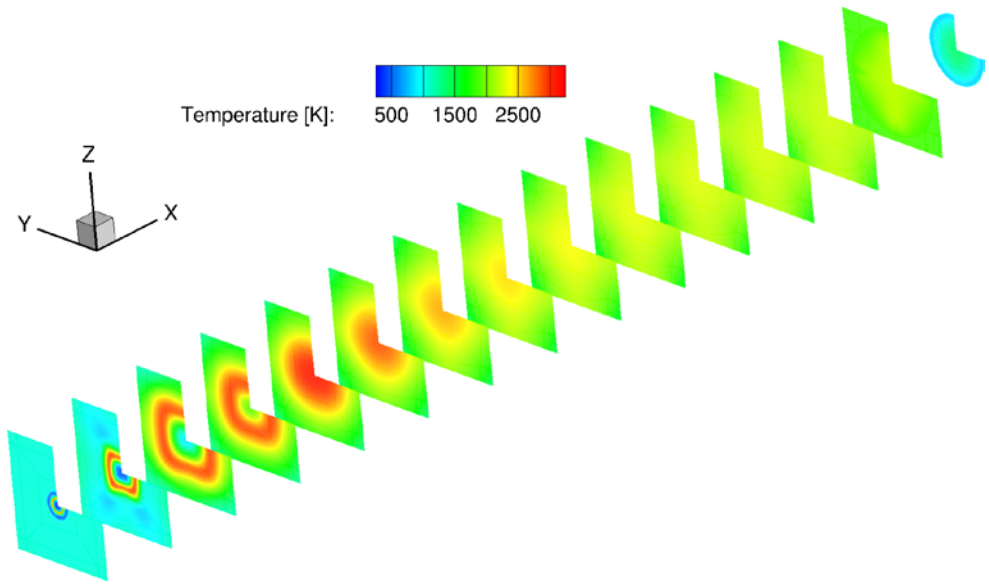

Figure 13: Mascotte 10 bar test case 3D simulation – temperature field slices at discrete axial positions.

4. ASTRIUM Subscale Chamber

4.1 Hardware and Test Data

The ASTRIUM subscale chamber test case was presented by Knab & Preclik [2] at the 3rd International Workshop on Rocket Combustion Modeling in Paris 2006. The calorimeter chamber, shown in Figure 14, consists of eleven independently water cooled segments in the cylindrical part and nine in the convergent-divergent nozzle section. It employs nineteen coaxial injection elements. The heat pick up of the water in the twenty segments has been used to determine the axial profile of the wall heat flux. The considered load point lies at a chamber pressure of $p_c = 100bar$ and a mixture ratio of $O/F = 6$ and hence is totally different from the load point of the Mascotte test case but comparable to the reference operating point of the Vulcain rocket engine. Oxygen is injected in transcritical state ($p > p_{crit}$, $T < T_{crit}$) and is treated by the Lagrangian droplet tracking module in Rocflam3. Hydrogen is injected in supercritical state. Both injection temperatures are around $T_{inj} \approx 100K$. As for the Mascotte test case, hydrogen is brought into the computational domain by the Lagrangian module but is immediately transferred to the Eulerian regime via source terms for mass, momentum and enthalpy. The mass flow rates are $\dot{m}_{ox} \approx 7.3\,kg/s$ and $\dot{m}_{fu} \approx 1.2\,kg/s$. The contraction ratio of the chamber is $\epsilon = 2.5$. The characteristic length is $l^* = 0.84m$. These two parameters are very similar to those of common rocket engines. Of course, this is not by accident – the chamber has been designed that way to generate experimental results that can be transferred to full scale rocket combustion chambers. As for the Mascotte combustor, coaxial injection elements are used. They exist of an oxygen tube and a hydrogen annulus. The oxygen tube is recessed but this is not taken into account by the simulation.
For this test case the focus lies on the correct computation of the wall heat flux profile which is available from the calorimetric heat flux measurements.

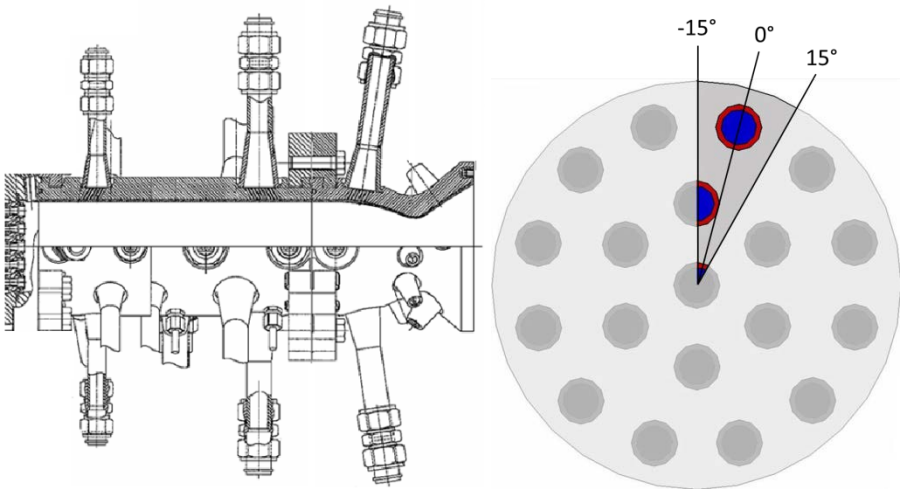

Figure 14: ASTRIUM subscale chamber - Left: Drawing of chamber and nozzle; Right: Injection element pattern. The colored part is the 30°-segment which can be treated in a three-dimensional simulation.

4.2 Simulation Settings

As for the for the Mascotte test case, the 2D/axisymmetric computations of the ASTRIUM subscale chamber are performed on a segment of one degree with one grid cell in circumferential direction. In axial direction, the cell width increases from $1mm$ at the faceplate to $2mm$. This value is kept constant down to the convergent part. In the convergent part, there is a refinement to $0.3mm$ in the throat area. In radial direction, the grid starts with a resolution of $0.4mm$ for the main flow and ends with a cell width of $0.6\mu m$ at the chamber wall, i.e. there is a strong refinement in the boundary layer. As the wall heat flux is the most important result for this test case it is assured that $y^+ < 1$ for the wall-adjacent grid cell. With the given dimensions, the grid consists of a total number of $321 \times 131 = 42 \cdot 10^3$ grid cells. It is shown in Figure 15.
Both the faceplate and the liner wall are modeled as no-slip walls. While the faceplate is assumed to be adiabatic, the temperature profile given in the test case description [2] is prescribed for the liner. Symmetry boundary conditions are applied in circumferential direction. A supersonic boundary condition is set on the outlet.
The injection element pattern cannot be reproduced exactly in two dimensions. Instead, the circular element rows have to be replaced by concentric rings. That does not make a difference for the central element but it is an

approximation for the two outer rows. In-house investigations suggest that it is important to maintain the distance between the outer row/ring and the wall in order to be able to compute the correct wall heat flux in the vicinity of the faceplate. That means that the width of the ring must be equal to the diameter of the injection elements. At the same time it is important that the propellants are injected with the correct momentum. To satisfy both constraints is possible using the Lagrangian droplet tracking module for propellant injection via source terms. This is done in the present simulation.

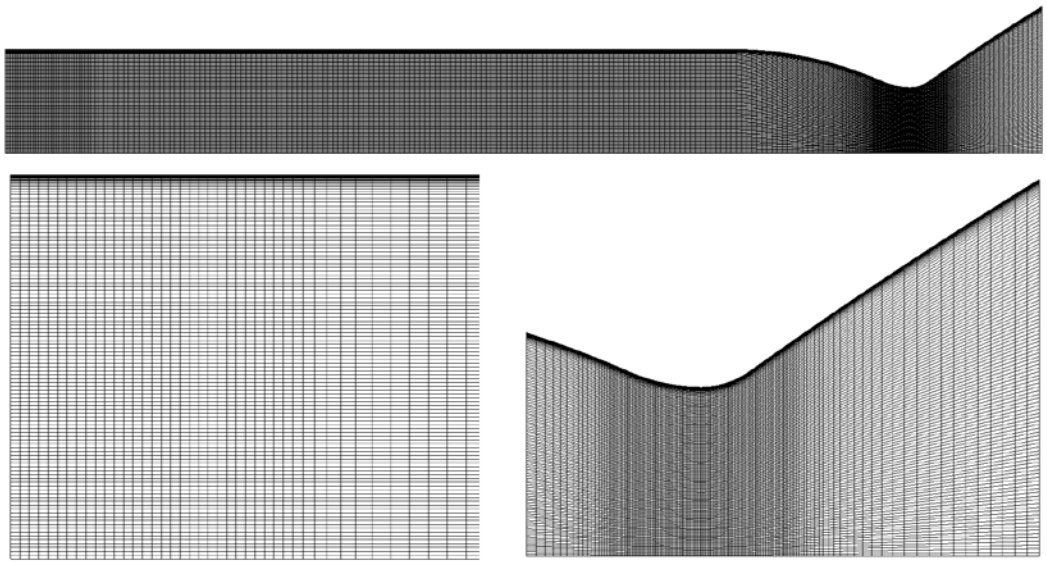

Figure 15: ASTRIUM subscale chamber 2D/axisymmetric simulation – computational grid (top: complete domain, bottom left: zoom on the inflow and faceplate region, bottom right: zoom on the throat region)

The oxygen droplet size distribution is modeled using a Log-Normal distribution with a mass mean diameter of $95\mu m$. In contrast to the Mascotte test case, the distribution is not given in the test case description but has been chosen by the authors of this work. The distribution is approximated using 25 discrete droplet sizes. The droplets enter the domain along 25 discrete vectors with different off-axis angles. The injection of the droplets is distributed over eight grid cells for the central injector and over sixteen grid cells for each of the two outer injectors. With these settings, the spray is modeled by 25000 representative trajectories each covering a certain number of real oxygen droplets.
For turbulence modeling, the two-layer k-ϵ turbulence model as described by Rodi [20] is used. Turbulent Prandtl and Schmidt numbers are set constant to $Pr_t = Sc_t = 0.6$ which is the standard setting in Rocflam-II simulations. This setting deviates from the setting used for the Mascotte test case but gives the best agreement with experimental data regarding the wall heat flux. Nevertheless, as the goal is to use the same combination of turbulent Prandtl and Schmidt numbers for all H_2/O_2 combustors, investigations regarding this will be performed in future work also taking into account experimental data from ASTRIUM flight hardware.

4.3 Simulation Results

4.3.1 2D/axisymmetric simulation

Figure 16 shows the temperature and mixture fraction fields for the 2D/axisymmetric simulation of the subscale chamber. The black lines mark the stoichiometric mixture fraction level. The hot combustion zones correlate with this mixture fraction. It is noticeable that the flame of the central injector is shorter than the flames belonging to the outer injection rings whose lengths are almost the same. Remembering that the central injector is the only one which is represented correctly by the axisymmetric approximation poses the question whether this relation can also be observed in three dimensions.

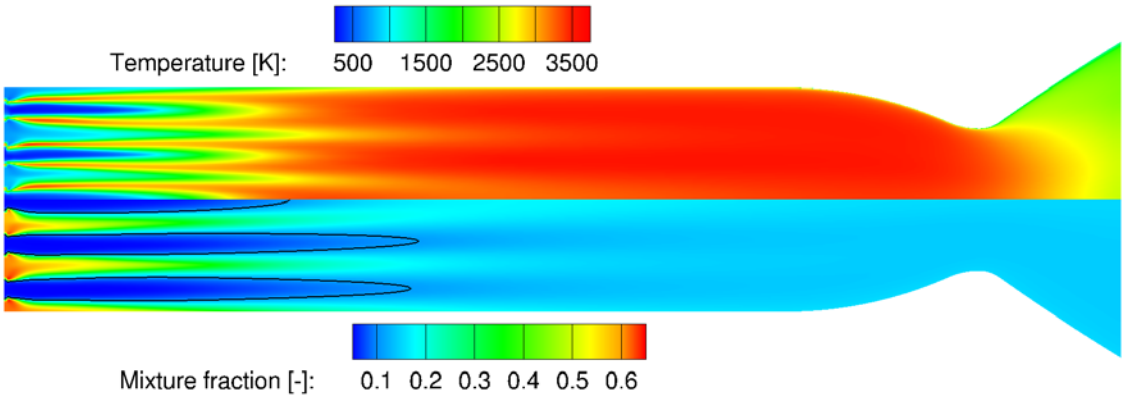

Figure 16: ASTRIUM subscale chamber 2D/axisymmetric simulation – temperature field (top) and mixture fraction (bottom). The black line marks the locations with stoichiometric mixture.

Figure 17 shows the non-dimensional specific wall heat flux computed by the axisymmetric simulation in comparison to the experimental data. The experimental data includes error bars for each calorimetric segment. The general agreement is satisfactory. However, there are some segments, where the numerical results do not fit with the experimental data very well. This is specifically notable in the vicinity of the faceplate, i.e. for the first two segments, where three-dimensional effects might play a role. However, it is also interesting that the simulation computes a decrease of the heat flux in the second half of the cylindrical part while the experimental data shows a slight increase. This topic shall also be addressed in future investigations.

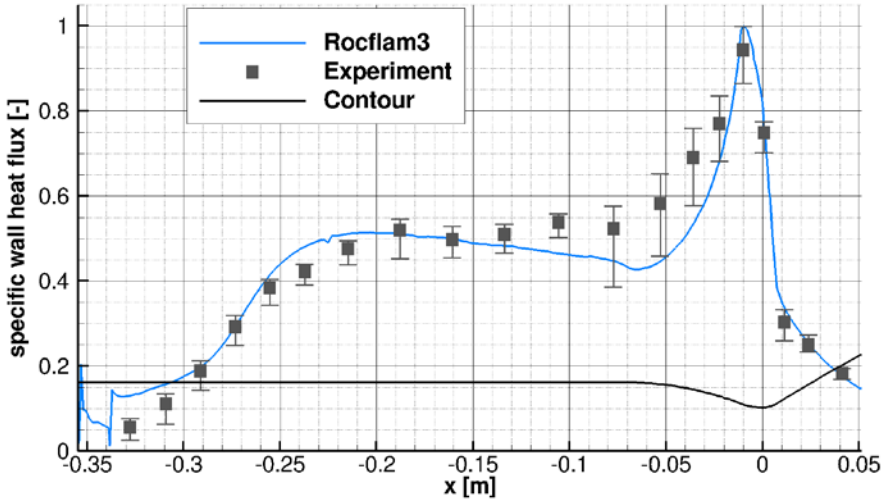

Figure 17: ASTRIUM subscale chamber 2D/axisymmetric simulation – non-dimensional specific wall heat flux

4.3.2 Three-dimensional simulation

The work on a three-dimensional simulation of a 30°-segment of the ASTRIUM subscale chamber is currently in progress. Unfortunately, it has not been possible to reach a converged solution for the three-dimensional simulation early enough to be shown in this paper. This is an important goal for future work.

5. Conclusion

Two subscale rocket combustors, namely the Mascotte 10 bar test case [1] and the ASTRIUM subscale chamber test case [2], have been investigated in two- and three-dimensional simulations using the newly developed CFD tool Rocflam3. The two-dimensional results show plausible behavior and good agreement with the experimental data.
While the numerical results for the Mascotte test case show very good agreement with the experimental OH emission image, the comparison with the measured mean temperatures leaves some open questions. The three-dimensional

simulation of the Mascotte test case shows good convergence and promising results. However, more detailed analyses will have to be performed to build up confidence regarding these results. Nevertheless, it is satisfying that grid resolution and model settings determined via two-dimensional simulations of the Mascotte test case also show good behavior in the corresponding three-dimensional simulation. This is important as it is not realistic to perform extensive parameter studies in three-dimensional simulations. Instead, parameters and settings shall be elaborated mainly via two-dimensional computations as they are much faster.
For the ASTRIUM subscale chamber test case where the focus is on the wall heat flux, the agreement between experimental data and simulation results is very good. While the three-dimensional simulation of this test case could not be finished in due time for this paper, the presented results for the Mascotte test case show that it is possible to simulate rocket combustion problems in both two and three spatial dimensions with the new CFD tool Rocflam3.
The final goal to be able to simulate full-scale multi-injector configurations in three dimensions in a predictive manner, i.e. with fixed settings, has not yet been reached but some important steps are taken now. The future work with Rocflam3 shall concentrate on the three-dimensional simulation of both single- and multi-injector subscale configurations before moving on to full-scale problems.

6. Acknowledgment

This work was performed within the national technology programs TARES and TEKAN 2010 II. These programs are sponsored by the German Space Agency, DLR Bonn, under contract No. 50RL1210 and contract No. 50RL0710, respectively.

7. References

[1] L. Vingert and M. Habiballah, "Test Case RCM-2: Mascotte single injector 10 bar," in *Proceedings of the 2nd International Workshop on Rocket Combustion Modeling - Atomization, Combustion and Heat Transfer*, Lampolshausen, 2001.

[2] O. Knab and D. Preclik, "RCM Test-Case RCM-3: "EADS-ST Subscale Chamber"," in *Proceedings of the 3rd International Workshop Rocket Combustion Modeling*, Paris, 2006.

[3] M. Frey, B. Kniesner and O. Knab, "Consideration of Real Gas Effects and Condensation in a Spray Combustion Rocket-Thrust-Chamber Design Tool," *Progress in Propulsion Physics - Volume 2,* pp. 285-296, 2011.

[4] H. Riedmann, B. Kniesner, M. Frey and C.-D. Munz, "Modeling of Combustion and Flow in a Single-Element GH2/GO2 Combustor," in *DLRK 2012*, Berlin, Germany, 2012.

[5] O. J. Haidn, Proceedings, 2nd International Workshop on Rocket Combustion Modeling, Atomization, Combustion and Heat Transfer, Lampoldshausen, Germany: DLR, 2001.

[6] D. Scherrer, F. Chedevergne, P. Grenard, J. Troyes, A. Murrone, E. Montreuil, F. Vuillot, N. Lupoglazoff, M. Huet, B. Sainte-Rose, P. Thorigny, N. Bertier, J. M. Lamet, T. Le Pichon, E. Radenac, A. Nicole, L. Matuszewski and M. Errera, "Recent CEDRE Applications," *Aerospace Lab Journal - Issue 2*, March 2011.

[7] M. Lempke, P. Gerlinger, M. Rachner and M. Aigner, "Euler-Lagrange Simulation of a LOX/H2 Model Combustor with Single Shear Coaxial Injector," in *High Performance Computing in Science and Engineering '10*, Berlin Heidelberg, Springer-Verlag, 2011, pp. 203-215.

[8] J.-F. Izard and A. Mura, "Lagrangian Modeling of Turbulent Spray Combustion: Application to Rocket Engines Cryogenic Conditions," in *Progress in Propulsion Physics 2*, Les Ulis, France, EDP Sciences, 2011, pp. 207-224.

[9] B. Ivancic, H. Riedmann and M. Frey, "Validation of Turbulent Combustion Models for 3D-Simulations of Liquid H2/O2 Rocket Combustors," in *Space Propulsion Conference*, Bordeaux, France, 2012.

[10] R. Farmer, R. Pike et G. Cheng, «CFD Analyses of Complex Flows,» *Computers and Chemical Engineering 29,* pp. 2386-2403, 2 September 2005.

[11] Y.-S. Chen, T. H. Chou, B. R. Gu, J. S. Wu, Y. Y. Lian und L. Yang, „Multiphysics Simulations of Rocket Engine Combustion,“ *Computers & Fluids 45,* pp. 29-36, 2011.

[12] S. Zurbach, Proceedings of the 3rd International Workshop on Rocket Combustion Modeling, Vernon, France: Snecma, Safran Group, 2006.

[13] B. Ivancic, M. Frey and O. Knab, "3D-Numerical Investigation of Turbulent Combustion and Heat Transfer Processes in H2-O2 Liquid Rocket Combustors," in *Space Propulsion Conference*, San Sebastian, Spain, 2010.

[14] M. Frey, T. Aichner, B. Ivancic, B. Kniesner and O. Knab, "Modeling of Rocket Combustion Devices," in *10th*

AIAA/ASME Joint Thermophysics and Heat Transfer Conference, Chicago, Illinois, USA, 2010.

[15] M. M. Masquelet, Simulations of a Sub-Scale Liquid Rocket Engine: Transient Heat Transfer in a Real Gas Environment: Masterthesis, Atlanta, Georgia, USA: Georgia Institute of Technology, 2006.

[16] S. V. Patankar und D. B. Spalding, „A Calculation Procedure for Heat, Mass and Momentum Transfer in Three-Dimensional Parabolic Flows,“ *International Journal of Heat and Mass Transfer, Vol. 15, Iss. 10*, pp. 1787-1806, October 1972.

[17] H. L. Stone, "Iterative Solution of Implicit Approximations of Multidimensional Partial Differential Equations," *SIAM Journal of Numerical Analysis, 5*, pp. 530-558, 1968.

[18] D. C. Wilcox, "Formulation of the k-omega Turbulence Model Revisited," in *45th AIAA Aerospace Sciences Meeting and Exhibit*, Reno, Nevada, USA, 2007.

[19] W. P. Jones and B. E. Launder, "The Prediction of Laminarization with a Two-Equation Model of Turbulence," *International Journal of Heat and Mass Transfer, vol. 15*, pp. 301-314, 1972.

[20] W. Rodi, „Experience with Two-Layer Models Combining the k-e Model with a One-Equation Model Near the Wall,“ in *29th Aerospace Sciences Meeting*, Reno, Nevada, USA, 1991.

[21] P. A. Durbin and B. A. Pettersson Reif, Statistical Theory and Modeling for Turbulent Flows, West Sussex, England: John Wiley & Sons Ltd., 2001.

[22] B. Kniesner, M. Frey and O. Knab, "Numerical Investigation of Gas Generator and Preburner Flows for Rocket Engine Applications," in *EUCASS*, St. Petersburg, Russia, 2011.

[23] B. Abramzon and W. A. Sirignano, "Droplet Vaporization Model for Spray Combustion Calculations," in *AIAA 26th Aerospace Sciences Meeting*, Reno, Nevada, USA, 1988.

[24] S. Candel, G. Herding, R. Snyder, P. Scouflaire, C. Rolon, L. Vingert, M. Habiballah, F. Grisch, M. Pealat, P. Bouchardy, D. Stepowski, A. Cessou and P. Colin, "Experimental Investigation of Shear Coaxial Cryogenic Jet Flames," *Journal of Propulsion and Power, Vol. 14, No.5*, pp. 826-834, September-October 1998.

[25] F. Grisch, P. Bouchardy and W. Clauss, "CARS Thermometry in High Pressure Rocket Combustors," *Aerospace Science and Technology, Volume 7, Number 4*, pp. 317-330, June 2003.

[26] F. Menter, J. Carregal Ferreira, T. Esch and B. Konno, "The SST Turbulence Model with Improved Wall Treatment for Heat Transfer Predictions in Gas Turbines," in *Proceedings of the International Gas Turbine Congress*, Tokyo, Japan, 2003.